Myeloid Sirtuin 6 Deficiency Causes Insulin Resistance in High-Fat Diet–Fed Mice by Eliciting Macrophage Polarization Toward an M1 Phenotype

Youngyi Lee,[1] Sun-O Ka,[1] Hye-Na Cha,[2] Yu-Na Chae,[3] Mi-Kyung Kim,[3] So-Young Park,[2] Eun Ju Bae,[4] and Byung-Hyun Park[1]

Diabetes 2017;66:2659–2668 | https://doi.org/10.2337/db16-1446

Obesity-related insulin resistance is closely associated with macrophage accumulation and subsequent cytokine release in local tissues. Sirtuin 6 (Sirt6) is known to exert an anti-inflammatory function, but its role in macrophages in the context of obesity has not been investigated. We generated myeloid-specific Sirt6 knockout (mS6KO) mice and investigated the metabolic characteristics after high-fat diet (HFD) feeding for 16 weeks. Compared with their wild-type littermates, HFD-fed mS6KO mice exhibited greater increases in body weight, fasting blood glucose and insulin levels, hepatic steatosis, glucose intolerance, and insulin resistance. Gene expression, histology, and flow cytometric analyses demonstrated that liver and adipose tissue inflammation were elevated in HFD-fed mS6KO mice relative to wild type, with a greater accumulation of F4/80$^+$CD11b$^+$CD11c$^+$ adipose tissue macrophages. Myeloid Sirt6 deletion facilitated proinflammatory M1 polarization of bone marrow macrophages and augmented the migration potential of macrophages toward adipose-derived chemoattractants. Mechanistically, Sirt6 deletion in macrophages promoted the activation of nuclear factor-κB (NF-κB) and endogenous production of interleukin-6, which led to STAT3 activation and the positive feedback circuits for NF-κB stimulation; this cross talk expedited an M1 polarization. We conclude that Sirt6 in macrophages is required for the prevention of obesity-associated tissue inflammation and insulin resistance.

Accumulation of macrophages in adipose tissue is positively correlated with body weight and causes insulin resistance in both humans and rodents (1). The increase in adipose tissue macrophages (ATMs) observed with obesity is also accompanied by macrophage phenotype shifts. Although alternatively activated M2 macrophages (F4/80$^+$CD11b$^+$CD11c$^-$) predominate in lean adipose tissue, the balance shifts toward proinflammatory M1 macrophages (F4/80$^+$CD11b$^+$CD11c$^+$) as obesity develops (2). M1 macrophages secrete a variety of proinflammatory cytokines and chemokines, including tumor necrosis factor (TNF)-α, interleukin-6 (IL-6), and MCP-1 (3). These cytokines activate inflammatory signaling pathways such as the inhibitor of κB kinase (IKK) and c-Jun NH_2-terminal kinase (JNK) pathways, which impair insulin activation of the phosphoinositide 3-kinase and Akt pathways (4). Similarly, activation of resident liver macrophages (Kupffer cells) and recruitment of circulating monocytes into the liver have been observed in animals fed a high-fat diet (HFD) and is causally implicated in the onset and progression of hepatic insulin resistance (5).

Sirtuin 6 (Sirt6), one of the seven mammalian sirtuins, is a nuclear protein and acts as an ADP-ribosyl transferase and NAD$^+$-dependent deacetylase (6). Sirt6 deacetylates histone H3 at lysine 9 (H3K9) and lysine 56 (H3K56), which results in chromatin condensation and decreased chromatin accessibility (7,8). Studies have suggested a beneficial role for Sirt6 in inflammation and metabolic stress. By deacetylating H3K9 on the promoters of nuclear factor-κB (NF-κB) target genes, Sirt6 alters chromatin structure to facilitate NF-κB destabilization at chromatin and termination of NF-κB signaling (9). Knockdown of Sirt6 in human

[1]Department of Biochemistry, Chonbuk National University Medical School, Jeonju, Jeonbuk, Republic of Korea
[2]Department of Physiology, College of Medicine, Yeungnam University, Daegu, North Gyeongsang, Republic of Korea
[3]Research Institute of Dong-A ST, Yongin, Gyeonggi, Republic of Korea
[4]College of Pharmacy, Woosuk University, Wanju, Jeonbuk, Republic of Korea
Corresponding authors: Eun Ju Bae, ejbae@woosuk.ac.kr, and Byung-Hyun Park, bhpark@jbnu.ac.kr.

Received 28 November 2016 and accepted 20 April 2017.

This article contains Supplementary Data online at http://diabetes.diabetesjournals.org/lookup/suppl/doi:10.2337/db16-1446/-/DC1.

See accompanying article, p. 2535.

umbilical vein endothelial cells increases the expression of proinflammatory cytokines (10), whereas overexpression of Sirt6 in mice is protective against metabolic pathologies caused by diet-induced obesity (11). In contrast, ablation of neural Sirt6 causes obesity (12). Additional evidence for the anti-inflammatory properties of Sirt6 has been provided in autoimmune disease and allergic airway inflammation models (13,14).

We and others have reported that myeloid-specific Sirt1 knockout (KO) mice develop tissue inflammation and insulin resistance upon exposure to an HFD (15,16). However, no study to our knowledge has investigated whether Sirt6 has a similar impact in macrophages or, more importantly, on how myeloid Sirt6 affects inflammatory and metabolic responses in mice under acute and chronic metabolic stress. With the aim of evaluating the influence of Sirt6 on macrophage infiltration and inflammation in local tissues of mice, we generated myeloid-specific *Sirt6* KO (mS6KO) mice. After feeding these mice a normal chow diet (NCD) or an HFD, we characterized tissue inflammation and glucose homeostasis. In addition, we studied the effects of Sirt6 on macrophage polarization and chemotaxis and their corresponding signaling pathways in isolated bone marrow macrophages (BMMs).

RESEARCH DESIGN AND METHODS

Animal Experiments

Sirt6$^{flox/flox}$ mice (B6;129-*Sirt6*^{tm1Ygu}/J) were crossed with *LysM-Cre* (B6.129P2-*lyz2*$^{tm1(cre)Ifo}$/J) mice to generate mS6KO mice (Supplementary Fig. 1*A*). Male mS6KO mice and age-matched littermates >6 weeks of age were fed ad libitum either an NCD or a 60% HFD (Research Diets, New Brunswick, NJ) for 16 weeks (Supplementary Table 1). The intraperitoneal glucose tolerance test (GTT) (1 g/kg of body weight) and insulin tolerance test (ITT) (0.5 units/kg of body weight) were performed after 16 and 6 h of fasting, respectively. A hyperinsulinemic-euglycemic clamp study (17), indirect calorimetry measurements (18), and stromal vascular fraction (SVF) isolation and FACS analysis (15) were performed as previously described. All experimental procedures were approved by the Institutional Animal Care and Use Committees of Chonbuk National University (permit no. CBNU 2015-090) (Jeonbuk, Republic of Korea) and Yeungnam University (permit no. YUMC-AEC2015-021) (Daegu, Republic of Korea).

Biochemical Analysis

Plasma levels of various cytokines and enzymes were measured by using specific ELISA kits (TNF-α, IL-1β, and IL-6 [Invitrogen, Carlsbad, CA]; insulin [Millipore, Billerica, MA]; MCP-1 [R&D Systems, Minneapolis, MN]; and aspartate aminotransferase [AST] and alanine aminotransferase [ALT] [Asan Pharmaceutical, Seoul, Republic of Korea]). For triglyceride (TG) quantification, liver tissues were homogenized and extracted in a mixture of chloroform, methanol, and distilled water (2:1:1). Liver TG concentrations were measured with a specific TG assay kit (Asan Pharmaceutical) and are expressed as milligrams of TG per 100 mg of liver tissue.

Histology

Fixed tissues were embedded in 10% formalin solution. Tissue sections (5 μm for liver and 7 μm for adipose tissue) were stained with hematoxylin-eosin (H-E) for light microscopy. Immunohistochemical staining was performed by using the EnVision system (DAKO, Carpinteria, CA). Sections were immunostained with antibodies against F4/80, CD11b (Abcam, Cambridge, U.K.), or perilipin (Fitzgerald, Acton, MA). Peroxidase activity was detected with 3-amino-9-ethyl carbazole. To assess morphological changes in liver, we used the nonalcoholic fatty liver disease (NAFLD) activity score (NAS), which includes histological features and has been defined as the unweighted sum of scores for steatosis (0–3), lobular inflammation (0–3), and ballooning (0–2) (19). The adipocyte area in selected fat tissue sections was measured by using iSolution DT 36 software (Carl Zeiss, Oberkochen, Germany). The number of crown-like structures (CLSs) was counted in 10 different high-power fields from each section.

Cell Culture and In Vitro Migration Assay

BMMs were obtained from bone marrow cells by cultivation for 6 days in α-minimum essential medium supplemented with 30% L929 conditioned medium (CM). For M1 or M2 differentiation, BMMs were treated with lipopolysaccharide (LPS) (10 ng/mL) + interferon-γ (IFN-γ) (50 units/mL) or IL-4 (10 ng/mL), respectively. To prepare 3T3-L1 CM for in vitro migration assay, fully differentiated 3T3-L1 cells were further cultured in migration media for 2 days, and the supernatants were harvested. For migration assays, BMMs from wild-type (WT) or mS6KO mice were pretreated with either Bay 11-7802 (Enzo Life Sciences, Farmingdale, NY), Stattic (Santa Cruz Biotechnology, Dallas, TX), or LMT-28 (a gift from S.S. Hong, Inha University, Incheon, Republic of Korea) for 3 h. Cell migration was analyzed by using transwell migration assay chambers (BD Life Sciences, Franklin Lakes, NJ) by adding adipocyte CM to the lower chamber. The DNA binding activity of STAT3 was detected by using a TransAM STAT3 Kit (Active Motif, Carlsbad, CA).

Western Blotting

Tissues and cells were homogenized in T-PER Tissue Protein Extraction Reagent or M-PER Mammalian Protein Extraction Reagent (Thermo Fisher Scientific, Waltham, MA). Homogenates (20 μg of total protein) were separated by SDS-PAGE and transferred to nitrocellulose membranes. Blots were probed with primary antibodies against HSP90 (Enzo Life Sciences), p-Akt, Akt, Sirt6, p-p65, p65, p-IKKα/β, IKKβ, p-JNK, JNK, p-extracellular signal–regulated kinase (ERK), ERK, p-p38, p38, p-STAT3, STAT3, p-inhibitor of κBα (p-IκBα), pyruvate kinase muscle isozyme M2 (PKM2), acetylated lysine (Cell Signaling, Beverly, MA), and actin (Sigma-Aldrich, St. Louis, MO). Immunoreactive bands were detected with an ImageQuant LAS 4000 imager (GE Healthcare Life Sciences, Pittsburgh, PA).

RNA Isolation and Real-time RT-PCR

Total RNA was extracted from frozen liver tissue by using TRIzol reagent (Invitrogen). First-strand cDNA was generated with oligo(dT) adaptor primers by reverse transcriptase (TAKARA BIO, Tokyo, Japan). Specific primers for each gene (Supplementary Table 2) were designed by using Primer Express software (Applied Biosystems, Foster City, CA). RT-PCR was performed by using a One-Step RT-PCR Kit (Invitrogen). PCR fragments were separated by electrophoresis on 2% agarose gels followed by staining with ethidium bromide.

Statistical Analysis

Data represent the mean ± SD. Statistical comparisons were by two-way ANOVA followed by Fisher post hoc analysis. The significance of differences between groups was determined by Student unpaired *t* test. $P < 0.05$ was considered significant.

RESULTS

Myeloid Sirt6 Deletion Leads to Glucose Intolerance in HFD-Fed Mice

To evaluate the functional role of myeloid Sirt6 in the development of obesity-associated tissue inflammation, we generated mS6KO mice. The deletion of *Sirt6* was confirmed by RT-PCR by using RNA harvested from mS6KO mouse BMMs (Supplementary Fig. 1*B*). mS6KO mice were fertile, with no apparent developmental defects. Six-week-old mS6KO mice and WT littermates were fed either an NCD or a 60% HFD for 16 weeks. Although the total food intakes were similar (Supplementary Fig. 2*A*), the mean body weight of mS6KO mice fed an HFD was significantly higher than that of WT mice from 4 weeks of HFD feeding (Supplementary Fig. 2*B*). To investigate the mechanism of increased weight gain in mS6KO mice, we analyzed the metabolic rates by using indirect calorimetry. Under the HFD condition, mS6KO mice showed lower respiratory quotient (VCO_2/VO_2) and energy expenditure than WT mice (Supplementary Fig. 2*C* and *D*), suggesting that reduction in resting metabolic rate might account for the obesity seen in mS6KO mice. Fasting glucose levels (Fig. 1*A*) as well as basal and stimulated insulin levels (Fig. 1*B*) were also higher in HFD-fed mS6KO mice than in WT mice, and mS6KO mice exhibited impaired glucose tolerance and insulin sensitivity compared with WT mice as assessed by GTT and ITT (Fig. 1*C* and *D*). Even between WT and mS6KO mice with similar body weights, mS6KO mice had higher fasting glucose levels and insulin intolerance (Supplementary Fig. 3).

To evaluate which tissues contribute to the increased insulin resistance in the HFD-fed mS6KO mice, a hyperinsulinemic-euglycemic clamp study was performed. During the clamp, glucose was maintained at ~6 mmol/L in both groups. The glucose infusion rate (GIR) was decreased by 65% in mS6KO mice compared with WT mice (Fig. 2*A*). Consistent with this finding, whole-body glucose turnover was decreased by 36% (Fig. 2*B*), confirming the development of insulin resistance with the HFD. Hepatic glucose

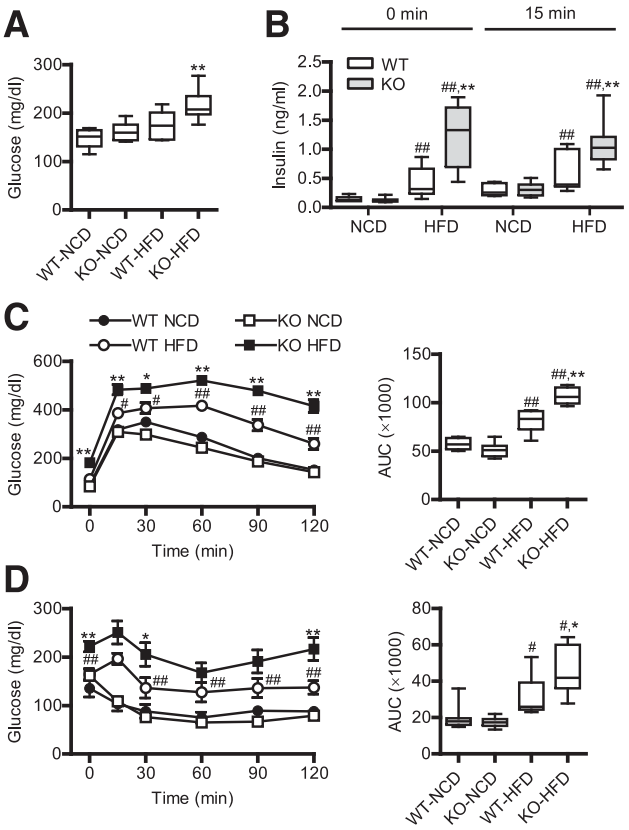

Figure 1—Metabolic characteristics of HFD-fed mS6KO mice. WT or mS6KO mice were fed either an NCD or an HFD for 16 weeks. *A*: Fasting plasma glucose levels. *B*: Basal and stimulated insulin levels. *C*: Intraperitoneal GTT plasma glucose concentrations. *D*: ITT plasma glucose concentrations. Areas under the curve (AUCs) were compared. Data are mean ± SD (n = 8). #$P < 0.05$, ##$P < 0.01$ vs. NCD-fed WT mice; *$P < 0.05$, **$P < 0.01$ vs. HFD-fed WT mice.

production (HGP) in the presence of insulin was significantly increased in mS6KO mice (Fig. 2*C*), and skeletal glucose uptake was reduced by 63% in mS6KO mice compared with WT mice (Fig. 2*D*). Increased insulin resistance in mS6KO mice was also confirmed by the finding that the levels of insulin-stimulated Akt Ser473 phosphorylation in liver, epididymal white adipose tissue (eWAT), and skeletal muscle were significantly lower in HFD-fed mS6KO mice than in WT mice, although these were similar between genotypes under NCD conditions (Fig. 2*E*). These results indicate that myeloid Sirt6 deletion causes systemic insulin resistance in HFD-fed mice, affecting insulin sensitivity in liver, eWAT, and skeletal muscle.

Myeloid Sirt6 Deletion Increases Inflammation in Liver and Adipose Tissue

The wet tissue weights, TG levels, and cholesterol content in the liver were significantly increased in HFD-fed mS6KO mice compared with HFD-fed WT mice, whereas little difference was observed between the genotypes under NCD conditions (Fig. 3*A*–*C*). Histological examination of liver sections showed increased lipid accumulation in

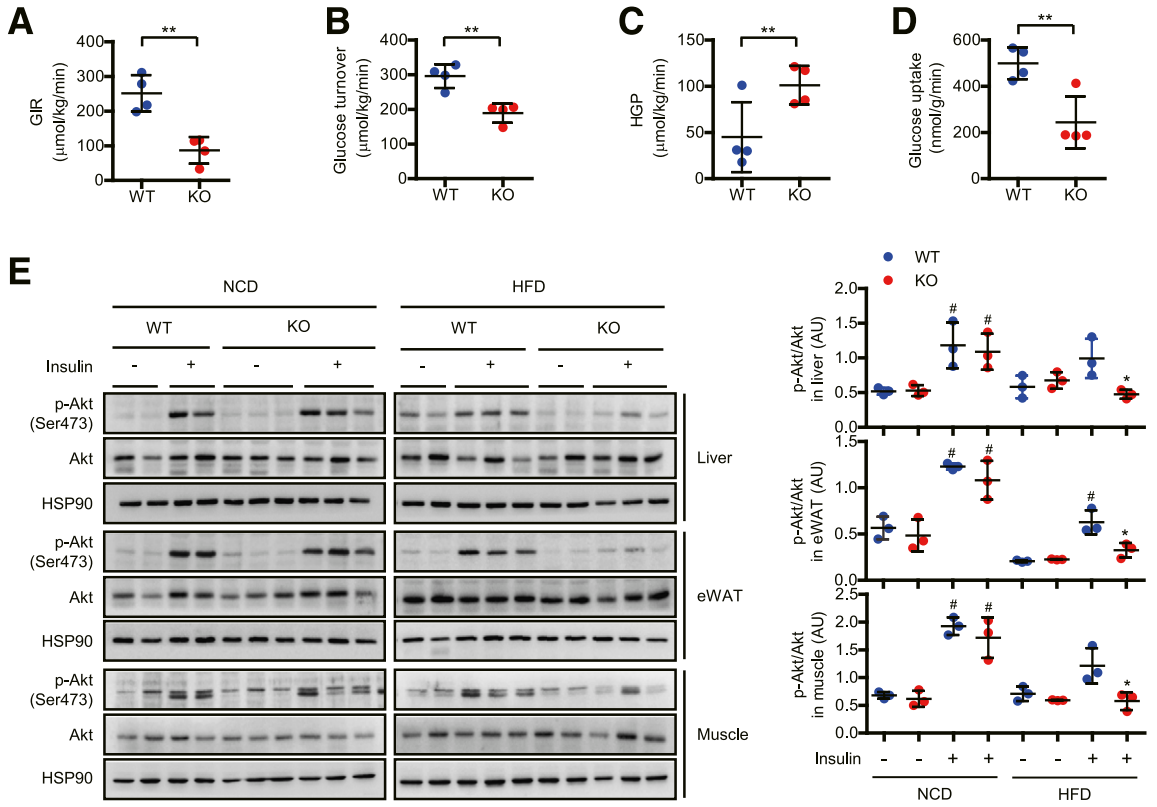

Figure 2—Worsening of insulin resistance in HFD-fed mS6KO mice. *A–D*: After 16 weeks on an HFD, the GIR, whole-body glucose turnover, HGP, and glucose uptake levels in the soleus muscle were determined during the hyperinsulinemic-euglycemic clamp test (n = 4). *E*: After 16 weeks on either an NCD or an HFD, liver-, adipose tissue–, and skeletal muscle–specific insulin sensitivity was measured by assessing the level of insulin-stimulated Akt phosphorylation. The intensities of the p-Akt and Akt immunoreactive bands were quantified (n = 3). Data are mean ± SD. #P < 0.05 vs. NCD-fed WT mice; *P < 0.05, **P < 0.01 vs. HFD-fed WT mice. AU, arbitrary unit.

HFD-fed mS6KO mice compared with HFD-fed WT mice (Fig. 3*D*). We next examined the inflammatory status, a key component in the pathogenesis of insulin resistance, in liver and adipose tissue. To assess macrophage infiltration into the liver, we immunostained liver sections with antibodies against F4/80. Compared with WT mice, HFD-fed mS6KO mice exhibited an increased number of F4/80$^+$ cells and liver damage as assessed by NAS (Fig. 3*D* and *E*). Real-time RT-PCR also confirmed the increased accumulation of proinflammatory macrophages in mS6KO mice compared with WT mice under HFD conditions, with increased expression of M1 macrophage genes (*F4/80*, *Cd11c*, *Cd11b*, *Ccl2*, *Ccr2*, *Tnfa*, *Il6*, *Il1b*, and *Icam1*), whereas M2 macrophage genes (*Arg1* and *Il10*) were reduced (Supplementary Fig. 4*A*). ELISA also revealed an increase of plasma cytokine levels in mS6KO compared with WT mice (Supplementary Fig. 4*B*). The extent of liver tissue damage in mS6KO mice, as assessed by increased plasma AST and ALT levels, correlated well with the degree of inflammation (Fig. 3*F*).

The tissue mass (data not shown) and the adipocyte size in eWAT significantly increased with HFD feeding, but no differences were observed between genotypes (Fig. 4*A* and *B*). ATMs often surround and ingest dying or dead adipocytes to form CLSs (20). We found that the number of CLSs per field in eWAT was significantly higher in mS6KO mice than in WT mice (Fig. 4*C*). FACS analysis of macrophage subpopulations in eWAT SVFs revealed that HFD-fed mS6KO mice exhibited a higher percentage of M1-like F4/80$^+$CD11b$^+$CD11c$^+$ cells than HFD-fed WT mice (Fig. 4*D*). In addition, the frequencies of CD8a$^+$ T cells were higher in HFD-fed mS6KO fat tissue (Fig. 4*D*).

Myeloid Sirt6 Deletion Enhances M1 Macrophage Features

In response to metabolic stress, ATMs polarize to proinflammatory M1-like cells (2). We first compared the levels of Sirt6 expression in eWAT of NCD- or HFD-fed mice and in M1/M2-polarized macrophages. Sirt6 expression was downregulated in eWAT of HFD-fed mice and in M1 macrophages but increased in M2 macrophages (Fig. 5*A*), supporting the in vivo anti-inflammatory effects of Sirt6. Because we identified that mS6KO fat tissue had the elevated level of M1 macrophages, we next studied the characteristics of M1-like macrophages in BMMs obtained from WT and mS6KO mice. The mRNA levels of M1 marker genes (e.g., *Ccl2*, *Tnfa*, *Nos2*, *Il1b*, and *Il6*) were markedly increased in M1 macrophages from mS6KO mice compared with those from WT mice (Fig. 5*B*). Accordingly,

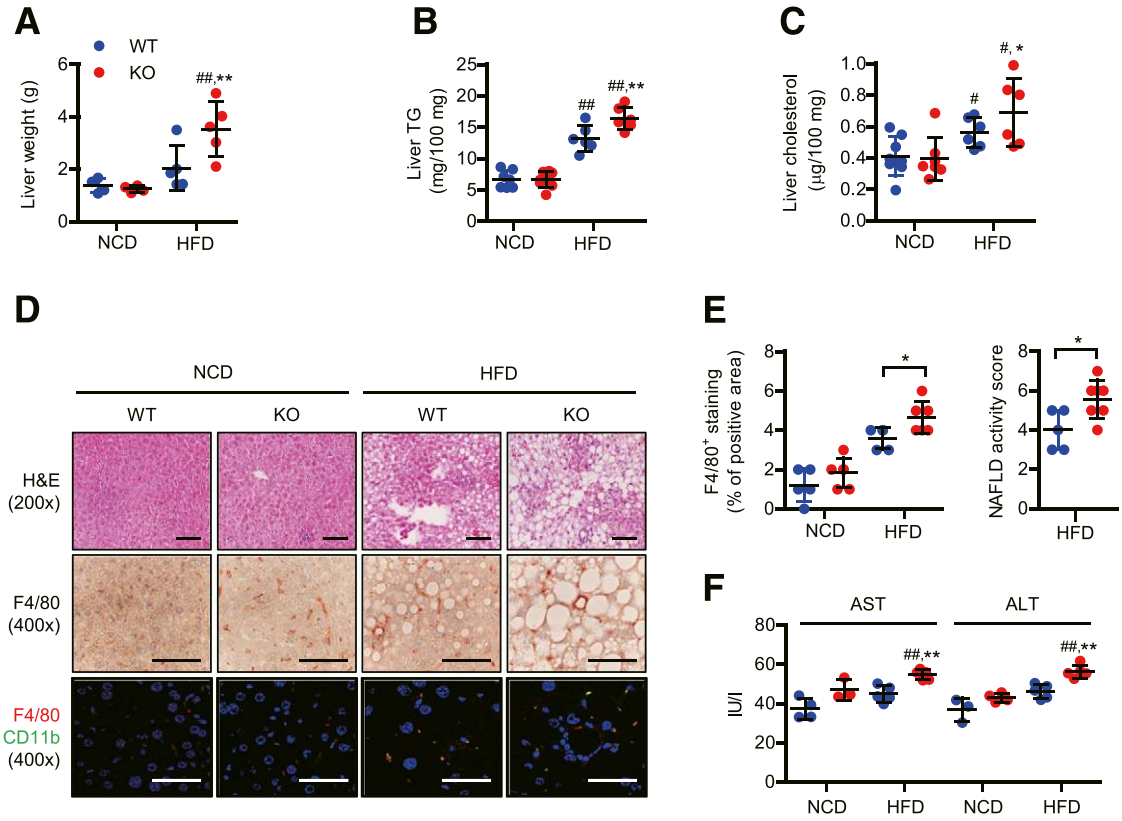

Figure 3—Effects of myeloid Sirt6 deletion on hepatic steatosis and macrophage infiltration. *A–C*: Liver tissues were retrieved after 16 weeks on either an NCD or an HFD, and their wet weights, TG levels, and cholesterol content were determined (n = 4–8). *D*: Liver sections were stained with H-E or immunostained with antibodies against F4/80 or CD11b. Scale bars = 250 μm. *E*: The numbers of F4/80$^+$ macrophages were counted and expressed as percentage of hepatocyte numbers. Inflammation index expressed as NAS was determined (n = 5). *F*: Plasma levels of AST and ALT were measured (n = 5). Data are mean ± SD. #P < 0.05, ##P < 0.01 vs. NCD-fed WT mice; *P < 0.05, **P < 0.01 vs. HFD-fed WT mice. IU, international unit.

the secretion of proinflammatory cytokines into the culture medium was markedly increased in LPS-treated BMMs from mS6KO mice compared with that from WT mice (Fig. 5*C*).

Activation of the NF-κB–IL-6–STAT3 Axis Is Involved in M1 Polarization

Activation of NF-κB and mitogen-activated protein kinases (MAPKs) has been implicated in the M1 phenotypic switch (21,22); therefore, we investigated the involvement of these signaling pathways in LPS-stimulated M1 polarization conditions. NF-κB activity, as assessed by p65 and IKKα/β phosphorylation, was increased in BMMs from mS6KO mice compared with those from WT mice (Fig. 5*D*). In addition, enhanced activation of p38 MAPK, but not JNK and ERK, was observed in BMMs from mS6KO mice, and we observed that LPS treatment induced increases in STAT3 phosphorylation (Fig. 5*D*) and STAT3 DNA binding activity (Fig. 5*E*) and that these changes were greater in mS6KO mice. A similar activation of NF-κB and STAT3 signaling was observed in the SVF of fat tissues of mS6KO mice (Fig. 5*F* and *G*). Together, these results suggest that NF-κB, p38 MAPK, and STAT3 signaling pathways mediate the M1 polarization shift of Sirt6-deleted macrophages.

Because LPS can activate NF-κB and thereby induce the production of IL-6, a major cytokine with a potentially important role in the induction of M1 marker expression through STAT3 activation (23,24), we hypothesized that endogenously produced IL-6 plays a role in STAT3 activation and the M1 polarization shift in mS6KO macrophages. To provide direct evidence for this idea, we blocked NF-κB signaling in LPS-stimulated BMMs by introducing a super-repressor (SR) form of IκBα that cannot be phosphorylated by IKKβ and, hence, functions as a stable inhibitor of NF-κB transcription factors (25). In mS6KO BMMs, IL-6 production, induction of an M1 marker gene (*Nos2*), and STAT3 phosphorylation were all inhibited by the SR to a similar level as those in WT cells (Fig. 6*A–C*), indicating that the increased NF-κB signaling played the role for M1 polarization in mS6KO mice. The role of STAT3 signaling in the enhancement of M1 polarization in mS6KO was also tested. When BMMs were pretreated with Stattic, a small-molecule inhibitor of STAT3, LPS-stimulated phosphorylations of not only STAT3 but also IKKα/β and p65 were reduced, implying the presence of cross talk between STAT3

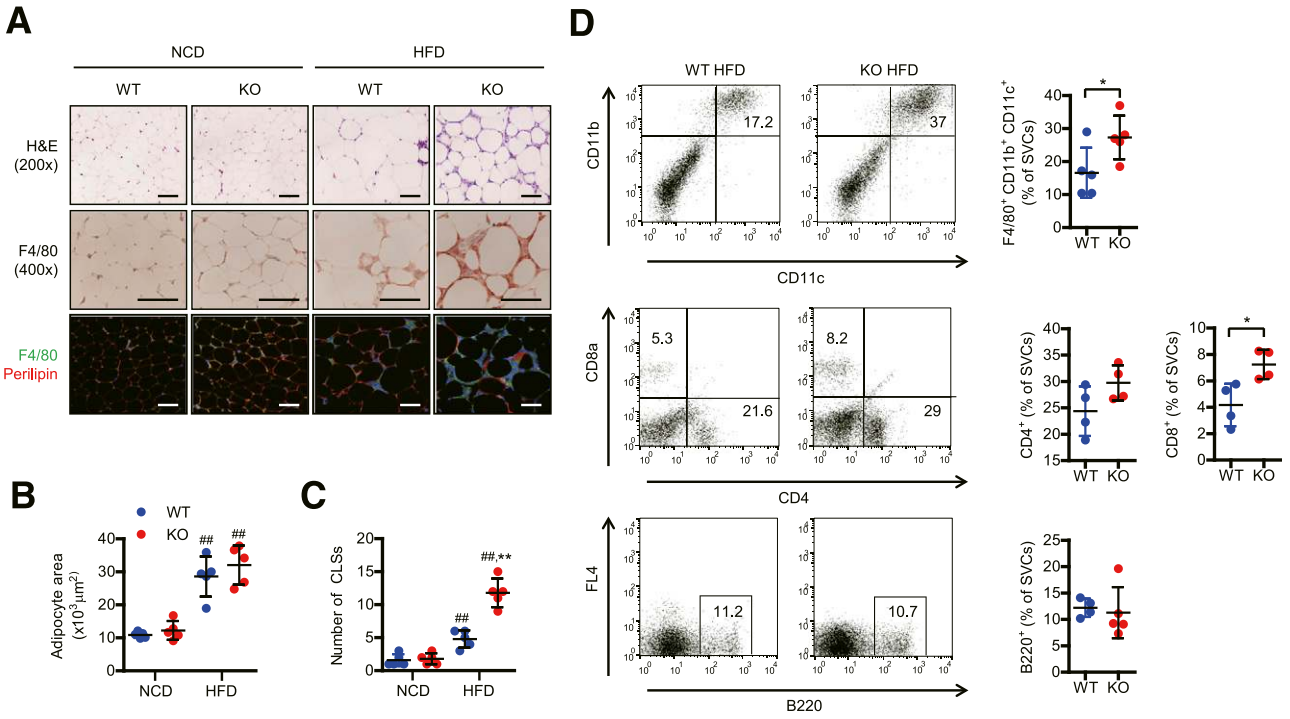

Figure 4—Effects of myeloid Sirt6 deletion on ATM infiltration. *A*: After 16 weeks on either an NCD or an HFD, eWAT sections were stained with H-E or immunostained with antibodies against F4/80 or perilipin. Scale bars = 250 μm. *B* and *C*: The mean adipocyte surface area and number of CLSs per field were determined (n = 5). *D*: The immune cell composition of the SVF prepared from eWAT was analyzed by FACS. The subpopulation of M1 macrophages (F4/80$^+$CD11b$^+$CD11c$^+$), T cells (CD4$^+$, CD8a$^+$), and B cells (B220$^+$) is expressed as the percentage of stromal vascular cells (SVCs) (n = 5). Data are mean ± SD. ##P < 0.01 vs. NCD-fed WT mice; *P < 0.05, **P < 0.01 vs. HFD-fed WT mice.

and NF-κB signaling pathways (Fig. 6*D*). Importantly, Stattic completely suppressed M1 marker gene expression, leading to no difference between genotypes (Fig. 6*E*). To test whether endogenously produced IL-6 is required for STAT3 activation in response to LPS treatment, we used LMT-28, a synthetic IL-6 receptor antagonist (26), and recombinant gp130 Fc chimera, an inhibitor of the IL-6 trans-signaling pathway (27). When BMMs were pretreated with these IL-6 signaling inhibitors before the LPS stimuli, STAT3 phosphorylation was markedly suppressed (Supplementary Fig. 5*A* and *C*). Indeed, LMT-28 suppressed the expression of M1 markers (Supplementary Fig. 5*B*), confirming the role of autocrine IL-6/STAT3 signaling. Taken together, these results support the idea that the M1 macrophage polarization shift by Sirt6 deficiency is mediated by activation of the NF-κB and the autocrine IL-6/STAT3 cascade.

Next, to further analyze the functional effects of Sirt6 deletion in macrophages, we performed transwell migration assays with BMMs. BMMs isolated from WT or mS6KO mice were layered onto a transwell insert, and migration was assessed with adipocyte CM present in the lower well. BMMs from mS6KO mice migrated faster than those from WT mice (Supplementary Fig. 6*A* and *B*). Whether the increased ability of chemotaxis of mS6KO BMMs is due to NF-κB and STAT3 activation also was tested. Pretreatment with Bay11-7802 (an NF-κB–specific inhibitor), Stattic, or LMT-28 markedly decreased BMM migration both in WT and KO cells, leaving KO cells with still-higher levels of migration relative to WT. These results suggest that Sirt6-deleted macrophages have the increased potential of migration through NF-κB and STAT3 activation in combination with a yet-unidentified mechanism.

Knowing that acetylated PKM2 phosphorylates STAT3 in the nucleus (28) and that PKM2 is deacetylated by Sirt6 (29), we hypothesized that Sirt6 would attenuate M1 polarization by deacetylating PKM2. To address this question, we overexpressed Sirt6 in intraperitoneal macrophages through adenovirus transduction and treated cells with LPS. LPS increased acetylation of PKM2 in macrophages, whereas Sirt6 overexpression lowered it to the basal level, possibly through direct interaction (Supplementary Fig. 7*A*). Pretreatment with shikonin, a PKM2 inhibitor, suppressed LPS-stimulated STAT3 phosphorylation (Supplementary Fig. 7*B*). These results suggest that Sirt6 deacetylates PKM2, preventing STAT3 from phosphorylation and thus leading to suppression of M1 polarization.

Finally, we reexpressed Sirt6 in KO BMMs to validate the requirement of Sirt6 for the suppression of M1 marker genes. Compared with AdLacZ-transduced BMMs, KO BMMs transduced with AdSirt6 exhibited decreased LPS-stimulated activation of the NF-κB and STAT3 signaling pathways and decreased expression of M1 marker genes (Supplementary Fig. 8*A* and *B*), confirming that Sirt6 uses the NF-κB and STAT3 pathways to alter M1 marker expression.

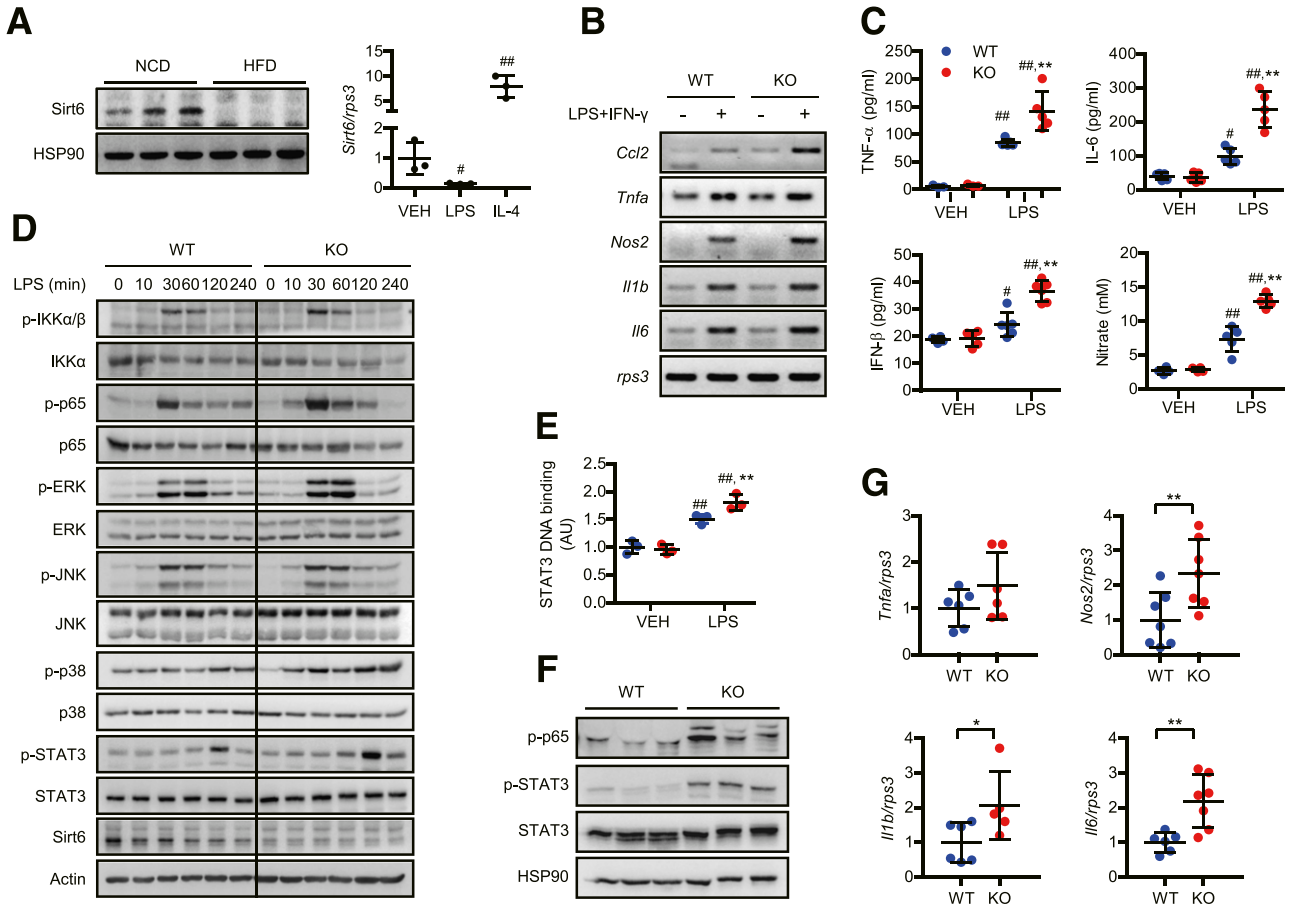

Figure 5—Regulation of macrophage polarization by Sirt6. BMMs were treated with either 10 ng/mL LPS and 50 units/mL IFN-γ (for M1 polarization) or 10 ng/mL IL-4 (for M2 polarization) for 24 h unless otherwise indicated. *A*: Sirt6 protein and mRNA levels in eWAT of NCD- or HFD-fed mice and in M1/M2-polarized macrophages were analyzed by Western blotting and real-time RT-PCR, respectively ($n = 3$). *B*: After M1 polarization, the expression patterns of M1 markers were compared by RT-PCR. *C*: BMMs from WT or mS6KO mice were treated with 10 ng/mL LPS for 2 h, after which the levels of secreted TNF-α, IL-6, and IFN-β, in addition to nitric oxide production, were determined ($n = 4$–6). *D*: Immunoblot analysis of whole-cell extracts from BMMs treated with 10 ng/mL LPS for the indicated periods. *E*: After treatment with 10 ng/mL LPS for 2 h, STAT3 DNA binding was analyzed ($n = 3$). *F* and *G*: Western blotting and real-time RT-PCR analyses of SVF from eWAT of HFD-fed mice ($n = 6$). Data are mean ± SD. #$P < 0.05$, ##$P < 0.01$ vs. nonstimulated; *$P < 0.05$, **$P < 0.01$ vs. WT. AU, arbitrary unit; VEH, vehicle.

DISCUSSION

We examined the effect of myeloid Sirt6 deletion on HFD-induced tissue inflammation and related metabolic disturbances in mice. We found that mS6KO mice are more susceptible to the development of diet-induced inflammation and insulin resistance than their corresponding WT littermates. In addition, mS6KO mice displayed an exacerbation of hepatic steatosis. Aggravation of insulin resistance in HFD-fed mS6KO mice was demonstrated by increased levels of fasting blood glucose and basal and stimulated circulating insulin, impaired GTT and ITT, and hyperinsulinemic-euglycemic clamp study results. The clamp study and Western blot analysis of Akt phosphorylation both indicated that all three major target tissues of insulin (liver, adipose tissue, and skeletal muscle) primarily contributed to the development of insulin resistance in HFD-fed mS6KO mice.

Monocyte/macrophage infiltration in adipose tissue and the polarization shift toward M1-like cells are main drivers of insulin resistance in the context of obesity (4), but the role of Sirt6 for macrophage migration and polarization in obesity settings remains elusive. In this study, we questioned whether myeloid Sirt6 deletion affects ATM accumulation and M1 polarization. Histological examination revealed that more than twofold higher levels of F4/80$^+$ macrophages forming CLSs accumulated in adipose tissue of HFD-fed mS6KO mice. In addition, FACS analysis of SVF obtained from HFD-fed mice showed that the subpopulation of M1-like macrophages (i.e., F4/80$^+$CD11b$^+$CD11c$^+$ cells), which are proinflammatory and have deleterious effects on insulin sensitivity (30), was increased in mS6KO mice.

Maintenance of the balance between M1 and M2 macrophages is essential for glucose homeostasis because the dominance of the M1 phenotype leads to the development of insulin resistance. Our conclusion that Sirt6 deficiency promotes macrophage phenotypic switch to a more proinflammatory M1 subtype was further substantiated by

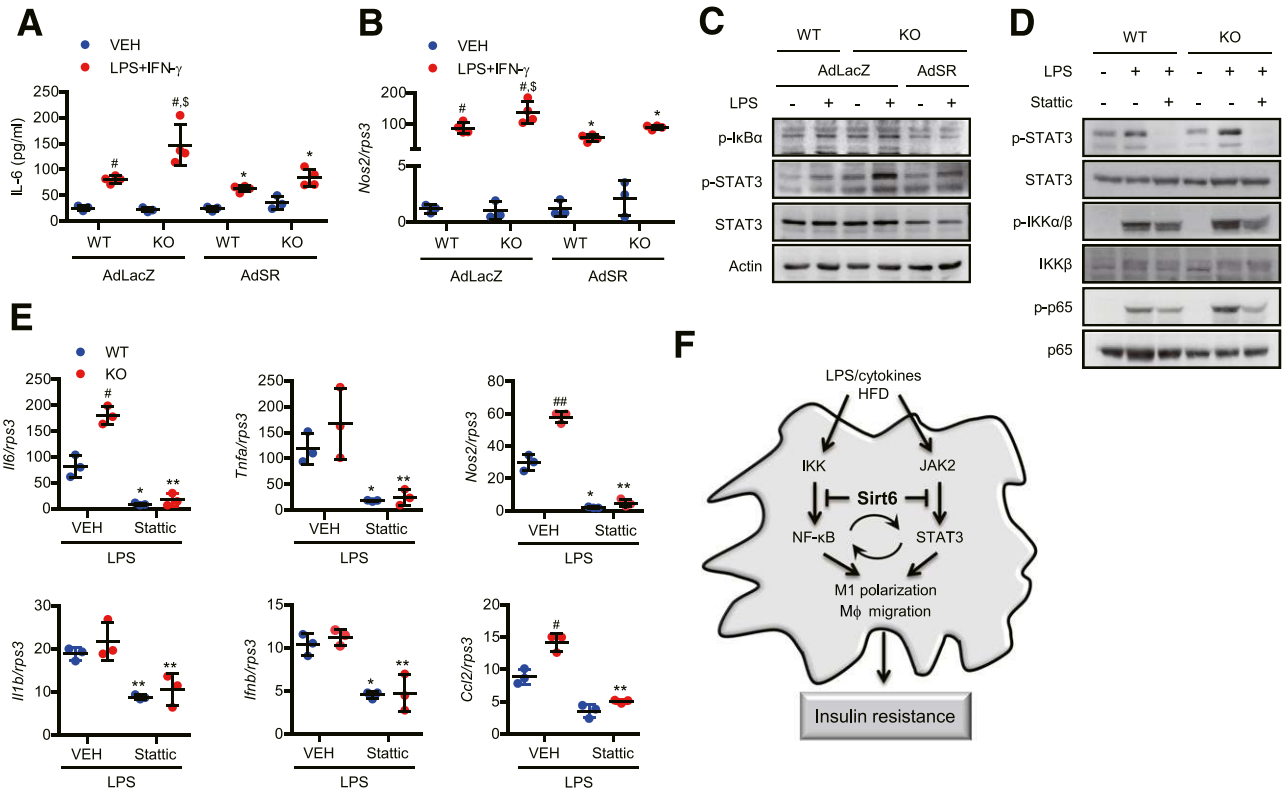

Figure 6—Regulation of the NF-κB/STAT3 signaling pathways by Sirt6. *A–C*: BMMs from WT or mS6KO mice were transduced with AdIκBαSR (AdSR) or AdLacZ and then treated with LPS (10 ng/mL) or LPS (10 ng/mL) + IFN-γ (50 units/mL) for 2 h. IL-6 production, *Nos2* expression, and NF-κB and STAT3 signaling pathways were analyzed. Data are mean ± SD (n = 3–4). #P < 0.05 vs. vehicle (VEH); \$$P$ < 0.05 vs. WT LPS + IFN-γ; *P < 0.05 vs. AdLacZ. *D* and *E*: BMMs from WT or mS6KO mice were treated with 10 ng/mL LPS for 2 h in the presence or absence of 5 μmol/L Stattic, a STAT3 inhibitor. The phosphorylations of STAT3 and IKK/p65 and M1 marker expression were analyzed by Western blotting and real-time RT-PCR, respectively (n = 3). #P < 0.05, ##P < 0.01 vs. WT VEH + LPS; *P < 0.05, **P < 0.01 vs. VEH + LPS. *F*: Schematic for the working model of myeloid Sirt6 control of macrophage (MΦ) polarization and migration for the regulation of insulin resistance.

the following findings. First, Sirt6 expression was lower in M1 macrophages and higher in M2 macrophages, which is consistent with a previous report that Sirt6 expression is reduced in peripheral blood mononuclear cells isolated from humans with the metabolic syndrome (31). Second, the mRNA levels of M1 marker genes and the secretion of proinflammatory cytokines were higher in M1 macrophages from mS6KO mice than in WT mice, whereas those of M2 marker genes were lower in M2 macrophages from mS6KO mice (data not shown).

To explore the underlying mechanism of this Sirt6 deficiency–mediated M1 polarization shift, we analyzed LPS-stimulated M1 polarization signaling pathways by using BMMs obtained from WT and mS6KO mice. After stimulation with LPS, the phosphorylations of IKK/NF-κB, p38 MAPK, and STAT3 were enhanced in Sirt6-deleted macrophages compared with WT cells. Previous studies have shown that the NF-κB–IL-6–STAT3 loop plays a pathological role in the occurrence of chronic inflammation (32–34). We thus tested the association between the NF-κB and STAT3 pathways during M1 polarization in Sirt6-deficient macrophages. The following pieces of evidence support the hypothesis that the cross talk between these two pathways is involved in Sirt6 regulation of M1 polarization. First, in LPS-stimulated BMMs, STAT3 activation occurs later than NF-κB activation as revealed in the time course analysis of NF-κB and STAT3 phosphorylation. Second, the IL-6 level was higher in the supernatants of mS6KO BMMs relative to WT, and abrogation of IL-6 trans-signaling with a small-molecule STAT3 inhibitor or IL-6 receptor antagonist down-regulated M1 marker genes in KO cells with dampening of the increase in STAT3 phosphorylation. These results suggest that IL-6 bridges the NF-κB and STAT3 pathways during M1 macrophage polarization. Third, BMMs transduced with IκBα SR exhibited decreased IL-6 production, STAT3 phosphorylation, and M1 marker expression. Overall, Sirt6 deletion likely led to the augmentation of NF-κB signaling by which IL-6 production was elevated in KO cells, and the subsequently elevated autocrine IL-6 signaling could trigger STAT3 phosphorylation to amplify the progression toward M1 polarization.

By using a transwell migration assay, we observed that mS6KO macrophages exhibited increased migration compared with WT macrophages in response to adipocyte-derived chemoattractants. These results suggest that myeloid Sirt6 regulates at least two stages of adipose

inflammation: *1*) macrophage infiltration (from circulatory monocytes to tissue macrophages) and *2*) macrophage subtype transformation (from monocytes to M1 or M2 subtype). These in vitro results correlated well with the in vivo data that showed marked increases in the number of the infiltrated F4/80$^+$ cells and the M1-like macrophage subpopulation in eWAT of HFD-fed mS6KO mice.

We also observed that myeloid Sirt6 deletion promoted accumulation or activation of F4/80$^+$ or CD11b$^+$ macrophages in the livers of HFD-fed mice. Consistently, gene expression analysis showed that the expression levels of numerous inflammatory genes were significantly elevated in the livers of HFD-fed mS6KO mice. Moreover, HFD-fed mS6KO mice showed increased hepatic steatosis compared with WT mice. These results suggest that the secretion of inflammatory cytokines from liver macrophages may impair insulin sensitivity of liver and affect hepatic lipid metabolism. For example, TNF-α can stimulate hepatic steatosis by promoting hepatocyte lipogenesis, ceramide production, and adipocyte lipolysis (35,36). This hypothesis is also supported by the finding that clodronate depletion of hepatic phagocytic cells/macrophages can markedly ameliorate hepatic steatosis and insulin resistance (37,38). In addition to TG accumulation and inflammation, hepatotoxicity and fibrosis are important features in the progression of NAFLD (39). We provide evidence that hepatotoxicity is greatly increased in HFD-fed mS6KO mice compared with WT mice, as indicated by the significantly higher blood levels of AST and ALT. Thus, mice deficient in myeloid Sirt6 are considerably prone to diet-induced NAFLD. The current finding that myeloid Sirt6 protects against diet-induced inflammation, insulin resistance, and liver steatosis highlights the significance of Sirt6 in macrophages as a therapeutic candidate for the metabolic syndrome, confirming the previous report that Sirt6 deficiency in immune cells is the cause of liver inflammation and progression to fibrosis in Sirt6 global KO mice (40).

In summary, the findings demonstrate that myeloid Sirt6 can affect the phenotypic switch and migration response of macrophages by modulating NF-κB and STAT3 pathways through autocrine IL-6 signaling (Fig. 6*F*). Given that M1 macrophage infiltration plays a critical role in systemic insulin resistance, regulation of myeloid Sirt6 might be a potential therapeutic strategy for the treatment of obesity-related metabolic diseases.

Funding. This work was supported by grants from the Medical Research Center Program (2008-0062279 and 2015R1A5A2009124) and by grants from the Basic Science Research Program (2017R1A2B2005730 and 2017R1A2B4008593) through the National Research Foundation, which is funded by the Korean government (Ministry of Science, ICT and Future Planning).

Duality of Interest. No potential conflicts of interest relevant to this article were reported.

Author Contributions. Y.L., S.-O.K., H.-N.C., Y.-N.C., M.-K.K., and S.-Y.P. conducted the experiments and analyzed the data. E.J.B. and B.-H.P. conceived the idea, designed the experiments, wrote the manuscript, and have primary responsibility for the final content. B.-H.P. is the guarantor of this work and, as such, had full access to all the data in the study and takes responsibility for the integrity of the data and the accuracy of the data analysis.

Prior Presentation. Parts of this study were presented in abstract form at the 77th Scientific Sessions of the American Diabetes Association, San Diego, CA, 9–13 June 2017.

References

1. Weisberg SP, McCann D, Desai M, Rosenbaum M, Leibel RL, Ferrante AW Jr. Obesity is associated with macrophage accumulation in adipose tissue. J Clin Invest 2003;112:1796–1808
2. Lumeng CN, Bodzin JL, Saltiel AR. Obesity induces a phenotypic switch in adipose tissue macrophage polarization. J Clin Invest 2007;117:175–184
3. Wensveen FM, Valentić S, Šestan M, Turk Wensveen T, Polić B. The "Big Bang" in obese fat: events initiating obesity-induced adipose tissue inflammation. Eur J Immunol 2015;45:2446–2456
4. Olefsky JM, Glass CK. Macrophages, inflammation, and insulin resistance. Annu Rev Physiol 2010;72:219–246
5. Lanthier N, Molendi-Coste O, Horsmans Y, van Rooijen N, Cani PD, Leclercq IA. Kupffer cell activation is a causal factor for hepatic insulin resistance. Am J Physiol Gastrointest Liver Physiol 2010;298:G107–G116
6. Kugel S, Mostoslavsky R. Chromatin and beyond: the multitasking roles for SIRT6. Trends Biochem Sci 2014;39:72–81
7. Michishita E, McCord RA, Berber E, et al. SIRT6 is a histone H3 lysine 9 deacetylase that modulates telomeric chromatin. Nature 2008;452:492–496
8. Michishita E, McCord RA, Boxer LD, et al. Cell cycle-dependent deacetylation of telomeric histone H3 lysine K56 by human SIRT6. Cell Cycle 2009;8:2664–2666
9. Kawahara TL, Michishita E, Adler AS, et al. SIRT6 links histone H3 lysine 9 deacetylation to NF-kappaB-dependent gene expression and organismal life span. Cell 2009;136:62–74
10. Lappas M. Anti-inflammatory properties of sirtuin 6 in human umbilical vein endothelial cells. Mediators Inflamm 2012;2012:597514
11. Kanfi Y, Peshti V, Gil R, et al. SIRT6 protects against pathological damage caused by diet-induced obesity. Aging Cell 2010;9:162–173
12. Schwer B, Schumacher B, Lombard DB, et al. Neural sirtuin 6 (Sirt6) ablation attenuates somatic growth and causes obesity. Proc Natl Acad Sci U S A 2010;107:21790–21794
13. Jang HY, Gu S, Lee SM, Park BH. Overexpression of sirtuin 6 suppresses allergic airway inflammation through deacetylation of GATA3. J Allergy Clin Immunol 2016;138:1452–1455.e13
14. Lee HS, Ka SO, Lee SM, Lee SI, Park JW, Park BH. Overexpression of sirtuin 6 suppresses inflammatory responses and bone destruction in mice with collagen-induced arthritis. Arthritis Rheum 2013;65:1776–1785
15. Ka SO, Song MY, Bae EJ, Park BH. Myeloid SIRT1 regulates macrophage infiltration and insulin sensitivity in mice fed a high-fat diet. J Endocrinol 2015;224:109–118
16. Schug TT, Xu Q, Gao H, et al. Myeloid deletion of SIRT1 induces inflammatory signaling in response to environmental stress. Mol Cell Biol 2010;30:4712–4721
17. Kwon MJ, Ju TJ, Heo JY, et al. Deficiency of clusterin exacerbates high-fat diet-induced insulin resistance in male mice. Endocrinology 2014;155:2089–2101
18. Chae YN, Kim TH, Kim MK, et al. Beneficial effects of evogliptin, a novel dipeptidyl peptidase 4 inhibitor, on adiposity with increased *ppargc1a* in white adipose tissue in obese mice. PLoS One 2015;10:e0144064
19. Kleiner DE, Brunt EM, Van Natta M, et al.; Nonalcoholic Steatohepatitis Clinical Research Network. Design and validation of a histological scoring system for nonalcoholic fatty liver disease. Hepatology 2005;41:1313–1321
20. Murano I, Barbatelli G, Parisani V, et al. Dead adipocytes, detected as crown-like structures, are prevalent in visceral fat depots of genetically obese mice. J Lipid Res 2008;49:1562–1568
21. Maa MC, Chang MY, Chen YJ, et al. Requirement of inducible nitric-oxide synthase in lipopolysaccharide-mediated Src induction and macrophage migration. J Biol Chem 2008;283:31408–31416

22. Yang C, Cao P, Gao Y, et al. Differential expression of p38 MAPK α, β, γ, δ isoforms in nucleus pulposus modulates macrophage polarization in intervertebral disc degeneration. Sci Rep 2016;6:22182
23. Greenhill CJ, Rose-John S, Lissilaa R, et al. IL-6 trans-signaling modulates TLR4-dependent inflammatory responses via STAT3. J Immunol 2011;186:1199–1208
24. Zhang C, Li Y, Wu Y, Wang L, Wang X, Du J. Interleukin-6/signal transducer and activator of transcription 3 (STAT3) pathway is essential for macrophage infiltration and myoblast proliferation during muscle regeneration. J Biol Chem 2013;288:1489–1499
25. Lee YR, Kweon SH, Kwon KB, Park JW, Yoon TR, Park BH. Inhibition of IL-1β-mediated inflammatory responses by the IkappaB α super-repressor in human fibroblast-like synoviocytes. Biochem Biophys Res Commun 2009;378:90–94
26. Hong SS, Choi JH, Lee SY, et al. A novel small-molecule inhibitor targeting the IL-6 receptor β subunit, glycoprotein 130. J Immunol 2015;195:237–245
27. Cron L, Allen T, Febbraio MA. The role of gp130 receptor cytokines in the regulation of metabolic homeostasis. J Exp Biol 2016;219:259–265
28. Lv L, Xu YP, Zhao D, et al. Mitogenic and oncogenic stimulation of K433 acetylation promotes PKM2 protein kinase activity and nuclear localization. Mol Cell 2013;52:340–352
29. Bhardwaj A, Das S. SIRT6 deacetylates PKM2 to suppress its nuclear localization and oncogenic functions. Proc Natl Acad Sci U S A 2016;113:E538–E547
30. Patsouris D, Li PP, Thapar D, Chapman J, Olefsky JM, Neels JG. Ablation of CD11c-positive cells normalizes insulin sensitivity in obese insulin resistant animals. Cell Metab 2008;8:301–309
31. de Kreutzenberg SV, Ceolotto G, Papparella I, et al. Downregulation of the longevity-associated protein sirtuin 1 in insulin resistance and metabolic syndrome: potential biochemical mechanisms. Diabetes 2010;59:1006–1015
32. Guo H, Jin D, Chen X. Lipocalin 2 is a regulator of macrophage polarization and NF-κB/STAT3 pathway activation. Mol Endocrinol 2014;28:1616–1628
33. Hung CC, Lin CH, Chang H, et al. Astrocytic GAP43 induced by the TLR4/NF-κB/STAT3 axis attenuates astrogliosis-mediated microglial activation and neurotoxicity. J Neurosci 2016;36:2027–2043
34. Kawashima T, Murata K, Akira S, et al. STAT5 induces macrophage differentiation of M1 leukemia cells through activation of IL-6 production mediated by NF-kappaB p65. J Immunol 2001;167:3652–3660
35. Bikman BT, Summers SA. Ceramides as modulators of cellular and whole-body metabolism. J Clin Invest 2011;121:4222–4230
36. Dressler KA, Mathias S, Kolesnick RN. Tumor necrosis factor-α activates the sphingomyelin signal transduction pathway in a cell-free system. Science 1992;255:1715–1718
37. Clementi AH, Gaudy AM, van Rooijen N, Pierce RH, Mooney RA. Loss of Kupffer cells in diet-induced obesity is associated with increased hepatic steatosis, STAT3 signaling, and further decreases in insulin signaling. Biochim Biophys Acta 2009;1792:1062–1072
38. Stienstra R, Saudale F, Duval C, et al. Kupffer cells promote hepatic steatosis via interleukin-1β-dependent suppression of peroxisome proliferator-activated receptor α activity. Hepatology 2010;51:511–522
39. Pais R, Charlotte F, Fedchuk L, et al.; LIDO Study Group. A systematic review of follow-up biopsies reveals disease progression in patients with non-alcoholic fatty liver. J Hepatol 2013;59:550–556
40. Xiao C, Wang RH, Lahusen TJ, et al. Progression of chronic liver inflammation and fibrosis driven by activation of c-JUN signaling in Sirt6 mutant mice. J Biol Chem 2012;287:41903–41913